Received: 17 September 2023 | Revised: 21 December 2023 | Accepted: 22 December 2023

DOI: 10.1002/bio.4675

RESEARCH ARTICLE

LUMINESCENCE The Journal of Biological and Chemical Luminescence WILEY

Amplified detection of SARS-COV-2 B.1.1.529 (Omicron) gene oligonucleotides based on exonuclease III-aided MoS_2/AIE nanoprobes

Gerile Oudeng[1] | Junguo Ni[2] | Hao Wu[3] | Honglian Wu[2] | Mo Yang[2] | Chunyi Wen[2] | Yuanwei Wang[1] | Hui Tan[1]

[1]Department of Hematology and Oncology, Shenzhen Children's Hospital, Shenzhen, Guangdong, China

[2]Department of Biomedical Engineering, The Hong Kong Polytechnic University, Hong Kong, SAR, China

[3]Department of Orthopedics, The Eighth Affiliated Hospital, Sun Yat-Sen University, Shenzhen, Guangdong, China

Correspondence
Yuanwei Wang and Hui Tan, Department of Hematology and Oncology, Shenzhen Children's Hospital, Futian, Shenzhen, Guangdong, 518026, China.
Email: yuanwei.wang@hotmail.com and huitan@email.szu.edu.cn

Funding information
This work was supported by the Natural Science Foundation of China (22304120, 22205095), the Science Technology Innovation Commission of Shenzhen Municipality (JCYJ20230807093800001, JCYJ20220530155415035, JCYJ20220818102804009, KQTD20210811090142053, JCYJ20220818103007014), Medical Scientific Research Foundation of Guangdong Province, China (B2023107), Guangdong High-level Hospital Construction Fund (2022-D4GRL).

Abstract

The coronavirus disease-2019 pandemic reflects the underdevelopment of point-of-care diagnostic technology. Nuclei acid (NA) detection is the "gold standard" method for the early diagnosis of the B.1.1.529 (Omicron) variant of severe acute respiratory syndrome-coronavirus disease-2. Polymerase chain reaction is the main method for NA detection but requires considerable manpower and sample processing taking ≥ 3 h. To simplify the operation processes and reduce the detection time, exonuclease III (Exo III)-aided MoS_2/AIE nanoprobes were developed for rapid and sensitive detection of the oligonucleotides of Omicron. Molybdenum disulfide (MoS_2) nanosheets with excellent optical absorbance and distinguishable affinity to single-strand and duplex DNAs were applied as quenchers, and aggregation-induced emission (AIE) molecules with high luminous efficiency were designed as donor in fluorescence resonance energy transfer-based nanoprobes. Exo III with catalytic capability was used for signal amplification to increase the sensitivity of detection. The composite nanoprobes detected the mutated nucleocapsid (N)-gene and spike (S)-gene oligonucleotides of Omicron within 40 min with a limit of detection of 4.7 pM, and showed great potential for application in community medicine.

KEYWORDS
aggregation-induced emission, amplified gene detection, fluorescence resonance energy transfer, molybdenum disulfide nanosheets, Omicron gene detection

1 | INTRODUCTION

In the past 2 years, coronavirus disease-2019 (COVID-19), produced by severe acute respiratory syndrome coronavirus 2 (SARS-CoV-2) infection, has evolved into a global epidemic and, as of September 2023, caused 6.95 million deaths worldwide [1–4]. In 2023, the World Health Organization discovered a variant of SARS-CoV-2, XBB.1.16, which was called "Omicron." The latter has a rapid growth trend and has emerged in 29 countries. In the past 2 years, researchers have explored different methods for detection of SARS-CoV-2 antigen/antibodies, such as electrochemical and field-effect transistor-based sensing technologies [5–7]. However, antigen tests are, in general, less sensitive than tests for nucleic acids (NAs) because antibody proteins cannot be amplified readily. Besides, in general, it takes 3–5 days

Gerile Oudeng and Junguo Ni contributed equally to this work.

to produce detectable antibodies in the body [8]. NA assays, such as the polymerase chain reaction (PCR), are considered to be the "gold standard" for the early diagnosis of COVID-19. The PCR assay is labor-intensive and time-consuming, so it poses challenges during a pandemic. Different methods of NA sensing, including electrochemical, localized surface plasmon resonance, and loop-mediated isothermal amplification, have been explored [9–11]. In our previous work, we investigated the feasibility of molybdenum disulfide (MoS_2) nanosheet-based array and an aggregation-induced emission luminogen (AIEgen)/graphene oxide nanocomposite for SARS-CoV-2-specific NA sequences [12, 13]. A simple-operated method of low-cost, large-scale availability is required, especially in communities with few medical resources. Few protocols have been reported on optimization of detection of NAs of Omicron.

In this work, a fluorescence resonance energy transfer (FRET) nanosensing method was developed to detect the NAs of Omicron. By monitoring the energy transfer between a donor and acceptor at the nanoscale, FRET technology can be employed to characterize virtually any biomolecular target from various clinical specimens [14]. The FRET performance is significantly regulated by the donors' optical properties. Traditional donor fluorophores usually suffer from aggregation-caused quenching (ACQ) effect in biological sensing environment, decreasing the intensity of fluorescence signal during the detection. In contrast, AIEgens are emerging as ideal candidates for their unique fluorescence amplification phenomenon when the intramolecular rotation or vibration is under restriction, which is termed as restriction of intramolecular rotation (RIR) mechanism [15, 16]. Among them, 2-(3-cyano-5,5-dimethyl-4-(4-[1,2,2-triphenylvinyl]styryl)furan-2(5*H*)ylidene)malononitrile (TPE-TCF) (TPET) possesses typical aggregation-induced emission (AIE)-features, with four benzene rings as free rotors providing sufficient motion [12, 17]. Besides, new types of acceptors, such as two-dimensional (2D) nanomaterials with unique optical quenching ability and large surface area for biomolecules interacting were highly concerned in recent studies [18, 19]. Among them, MoS_2 nanosheets with excellent biocompatibility and nanoscale-surface energy transfer effect have emerged as candidates [20–22]. However, few studies have explored how to effectively interact the novel FRET donor of AIE with the 2D nanomaterials and improve the virus NA sensitivity.

Here, we constructed 2D MoS_2 nanosheets and AIEgen TPET-based FRET nanoprobes aided by the enzyme exonuclease III (Exo III) for rapid and sensitive detection of the mutated nucleocapsid (N)-gene and spike (S)-gene oligonucleotides (oligos) of Omicron. Due to the distinguishable affinity from MoS_2 to single-stranded DNA (ssDNA) and duplex DNA, MoS_2 nanosheets can adsorb TPET-labeled single-strand capture probes selectively and quench their fluorescence [21, 23]. When exposed to a positive sample, TPET-labeled capture probes can hybridize with target genes to form duplex DNAs. Capture probes exposed to blunt-ended 3′ termini in duplex DNAs can be hydrolyzed stepwise by Exo III and release free targets to enter the next cycle. Through multiple recycling, the recycled targets ensure the full utilization of all invested probes, which leads to a considerable accumulation of free TPET labels in the environment, realizing a secondary amplification of fluorescence signals. MoS_2 nanoprobes could offer sensitivity, low expense for fabrication, and simple operation, and could be used in community medicine.

2 | MATERIALS AND METHODS

2.1 | Materials and reagents

MoS_2 material was purchased from XFNANO Materials Tech Co (Nanjing, China). Exo III (*Escherichia coli*) and NE Buffer™ (10×) were obtained from New England Biolabs (Ipswich, MA, USA) and stored at −20°C. Hydrochloric acid (37%) was sourced from VWR Chemicals (Radnor, PA, USA). UltraPure™ Tris–HCl (1 M, pH 7.5) was purchased from Invitrogen (Carlsbad, CA, USA). SYBR™ Gold Nucleic Acid Gel Stain (10,000× concentrate in dimethyl sulfoxide), O'RangeRuler 10 bp DNA Ladder, Orange DNA Loading Dye (6×), UltraPure DNase/RNase-Free distilled water, and TBE buffer (Tris−borate−EDTA, 10×) were from Thermo Fisher Scientific (Waltham, MA, USA). Regular Agarose G-10 was obtained from Shanghai Baygene Biotechnology (Shanghai, China) and stored at room temperature. Sodium chloride (≥ 99.5%) was purchased from Shanghai Aladdin Biochemical Technology (Shanghai, China) and stored at room temperature. All the gene sequences of capture probes, targets, and mismatched targets were synthesized and purified (high-performance liquid chromatography) by Sangon Biotech (Shanghai, China). The ReverTra Ace TM qPCR RT Kit for reverse transcription was purchased from Toyobo (Beijing, China). All these gene oligos were stored in ultrapure DNase/RNase-free deionized (DI) water at −4°C and diluted with Tris–HCl buffer (10 mM, pH 7.5) for further use.

2.2 | Prepration of the nanoprobe components

MoS_2 material was sonicated for 5 min in an ice bath (to exfoliate the nanosheets) and centrifuged at 2000 rpm for 5 min at room temperature (to remove aggregated particles). Then the nanosheets dispersion was dialyzed with a filter membrane (3500D in molecular weight) at least for 1 day to remove the lithium hydroxide [21]. The final MoS_2 nanosheets were stored at −4°C until further use. TPET was synthesized according to a previous method [24]. The sequences of all applied oligos are listed as following, 28354 Probe-N_{del} (P_N): 5'-ATGGTGCGGCGCGATC-3′ (OM185476.128279 to 28299); 22206 Probe-S_{del} (P_S): 5'-GTGCGTGAGCCAGAAGATCTCC-3′ (LC666933.111292 to 11318); Target-Influenza A (M gene) (T_{IA}): 5'-CTC GGC TTT GAG GGG GCC TGA-3′; Target-Influenza B (HA gene) (T_{IB}): 5'-GCC ATA GGA AAT TGC CCA ATA TGG GTG-3′.

TPET molecules were labeled on the 5′ terminals of the capture probes by covalent binding between the aldehyde group from TPET and amino group from probe; 150 μM capture probes in sodium borate buffer (1 mL, pH 8.5) were mixed with 100 μM TPET dispersion (1 mL, tetrahydrofuran). The mixture was stirred in the dark

overnight at room temperature and then purified via a dialysis process (molecular weight cut-off 1 kDa). TPET-probe products were lyophilized and kept at −20°C for further using.

2.3 | Characterization

The morphology of MoS_2 nanosheets was observed by transmission electron microscopy (TEM) using a 2100F system (Jeol, Tokyo, Japan). The hydrodynamic size and zeta potential of MoS_2 nanosheets were characterized by a Zetasizer Nano Z setup (Malvern Instruments, Malvern, UK). X-ray diffraction (XRD) spectroscopy was undertaken using an X-ray diffractometer (SmartLab; Rigaku, Tokyo, Japan). Optical absorbance spectroscopy was done on a ultraviolet-visible (UV-vis) spectrophotometer (Ultrospec™ 2100 Pro; MilliporeSigma, Burlington, MA, USA). Morphology was investigated based on atomic force microscopy (AFM) using Nanoscope™ IV (Digital Instruments, Tonawanda, NY, USA). All solutions used in gel electrophoresis were prepared with DI water from a water-purification system (Merck, Whitehouse Station, NJ, USA). Assays to measure fluorescence signals were conducted by a spectrophotometer (FLSP920; Edinburgh Instruments, Edinburgh, UK) containing a 450-W xenon lamp (Edinburgh Instruments).

2.4 | Gel electrophoresis

The sequences of target oligos comprised the N gene with its 28,362–28,371 positions deleted (T_N) and the S gene with its 22,194–22,196 positions deleted (T_S) of Omicron. The capture probes of T_N and Ts were labeled by TPET (denoted as "P_N" and "P_S") respectively. A 4% agarose gel was applied to verify the catalytic effect of Exo III on ssDNA and duplex DNA. Initially, 2 g of agarose was added to 50 mL of 0.5× TBE buffer and heated in a seal for 1 min in a microwave oven. The agarose gel was shaken intermittently and cooled down to 70°C. Then, SYBR™ Gold Nucleic Acid Gel Stain (5 μL) was added. Gel of thickness 0.5 cm was solidified and transferred to an electrophoresis tank. Samples of P_N (400 nM), T_N (200 nM), P_N (400 nM) + T_N (200 nM) with and without Exo III treatment were added to the gel in turn. Then, electrophoresis was carried out at a constant voltage of 110 V for 45 min in 0.5× TBE buffer and imaged under light (Alexa 488).

2.5 | Establisment of Exo III-aided MoS_2/AIE nanoprobes

To investigate the quenching effect of MoS_2, samples of P_N (20 nM), P_N (20 nM) + T_N (5 nM), and P_N (20 nM) + T_N (5 nM) treated by Exo III (0.015 U μL^{-1}) were incubated with MoS_2 nanosheets (120 μg mL^{-1}) for 20 min at room temperature, respectively. Then, the fluorescence intensity (FI) of each sample was characterized by photoluminescence (PL) spectroscopy in which TPET emission was recorded at 600–850 nm under excitation of 480 nm. To ascertain the amount of Exo III needed for sufficient catalysis, duplex DNAs of $P_N + T_N$ (20 nM:5 nM) were treated with Exo III (0.005, 0.01, 0.015, or 0.02 U μL^{-1}) for 40 min at 37°C. Then, the time needed for Exo III to carry out catalysis was determined by treating the duplex DNAs of $P_N + T_N$ with Exo III (0.015 U μL^{-1}) at 37°C for 0, 20, 40, 60, or 100 min. The fluorescence signals of each sample were analyzed quantitatively by PL spectroscopy. The sensitivity of Exo III-aided MoS_2 nanoprobes was investigated by incubating P_N (20 nM) with T_N (0, 0.01, 0.05, 0.1, 0.15, 0.3, 0.5, 1.0, 1.5. 2.5, or 5.0 nM) in Tris–HCl buffer (20 mM) according to the previous methods [25, 26]. Then, Exo III (0.015 U μL^{-1}) and MoS_2 nanosheets (120 μg mL^{-1}) were added and allowed to react for 40 min at 37°C. The relationship between $(F_t - F_{nt})/F_{nt}$ (where F_t represented the FI of P_N incubated with T_N and treated with MoS_2 and Exo III, and F_{nt} represented the FI of P_N treated with MoS_2 and Exo III) and the logarithm concentration of T_N were analyzed quantitatively. The limit of detection (LOD) was calculated as the ratio of three-times the standard deviation of the blank signal to the slope of the calibration curve ($3\sigma/S$).

2.6 | Sensing specificity of Exo III-aided MoS_2/AIE nanoprobes

To analyze the specificity of Exo III-aided MoS_2/AIE nanoprobes, P_N (20 nM) was incubated with T_N (1.0 nM), scrambled target sequence (T_{SC}), target-Influenza A (M gene) (T_{IA}), or target-Influenza B (haemagglutinin gene) (T_{IB}) in Tris–HCl (20 mM), then all samples were treated with Exo III (0.015 U μL^{-1}) and MoS_2 nanosheets (120 μg mL^{-1}) for 40 min at 37°C. Similar experiments were undertaken for specificity analyses of T_S detection by incubating P_S with T_S, T_{SC}, T_{IA}, T_{IB} and reacting at the conditions stated earlier.

3 | RESULTS AND DISCUSSION

3.1 | Sensing mechanism of Exo III-aided MoS_2/AIE nanoprobes for identification of the NAs of Omicron

We investigated the feasibility of using Exo III-aided MoS_2/AIE nanoprobes for the rapid and sensitive detection of gene oligos of Omicron. Figure 1a shows the target N genes and S genes of Omicron in which the deletions positioned at 28,362–28,371 in the N gene and 22,194–22,196 in the S gene were identified as being unique for Omicron according to global phylogenetic analyses [2]. The selectivity of these two deleted gene segments for identification of suspected-Omicron samples have been verified [3]. Therefore, in this work, an Exo III-aided MoS_2/AIE nanoprobe was designed to detect the deleted N-gene oligos (T_N) or deleted S-gene oligos (T_S) of Omicron sensitively. The capture probe was labeled with the red fluorescent TPET (Figure 1b). Furthermore, T_N/T_S could hybridize with their specific capture probes (P_N/P_S) and form duplex DNAs with strong

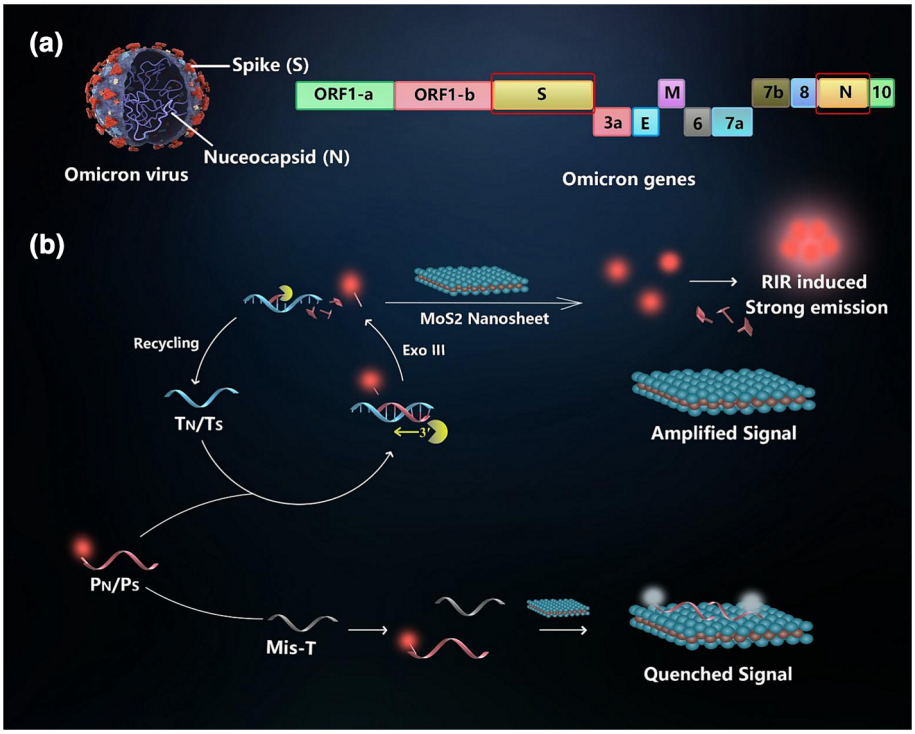

FIGURE 1 (a) Schematic of the targeting S or N genomic regions in SARS-CoV-2 B.1.1.529 (Omicron variant). (b) Schematic of Exo III-aided MoS_2/AIE FRET nanoprobes for amplified detection of T_N and T_S.

fluorescence. To increase the sensitivity of detection, Exo III was introduced into MoS_2-based nanoprobes due to its flexible catalysis. Exo III rarely catalyzes a free mononucleotide, instead it can hydrolyze the mononucleotide stepwise from its blunt-ended 3′ termini in duplex DNAs [27, 28]. Herein, P_N/P_S were complementary to T_N/T_S, respectively, and could form duplex DNAs with a blunt-ended 3′ terminus only on capture probes [29].

In the absence of targets (Figure 1b, bottom), hydrophilic P_N/P_S with low fluorescence emission would be adsorbed by MoS_2 nanosheets via van der Waals force between the basal planes of MoS_2 and the nucleobases of single-strand capture probes [30, 31]. Due to the optical absorbance of MoS_2 nanosheets, the fluorescence of TPET was quenched via FRET. However, in the presence of target T_N/T_S (Figure 1b, top), P_N/P_S hybridized with their specific targets to form duplex DNAs, which could not be absorbed by MoS_2 nanosheets. The blunt-ended 3′ termini of capture probes (P_N/P_S) in the hybridized duplex DNAs would be degraded by Exo III leading to the loss of the hydrophilic portion. The released hydrophobic TPET molecules aggregated to trigger the enhanced fluorescence via an RIR effect [31, 32]. By monitoring the change in the fluorescence signal, multiple Omicron-gene oligos could be detected sensitively.

3.2 | Characterization of MoS_2 nanosheets

MoS_2 nanosheets were exfoliated in aqueous via continuous sonication to obtain the 2D nanosheets with mono or few layers. The synthesized MoS_2 nanosheets had a thin-layered morphology according to TEM (Figure 2a). The thickness of MoS_2 nanosheets was around 2 nm according to AFM images, which matched their crystalline thickness of two or few layers (Figure 2b,c) [30]. High-resolution TEM image showed a lattice like morphology on the surface of MoS_2 (Figure 2d). Further, diffraction peaks at 14.40° (2θ) were indexed as (002) in the XRD pattern of layered MoS_2 nanosheets (Figure 2e) [21, 33]. In UV-vis absorbance spectra (Figure 2f), TPET-labeled probe (TPET-probe) showed the characterization peaks of TPET at 360 and 480 nm, indicating the coupling of TPET and capture probes. MoS_2 nanosheets showed negatively charged zeta potential at −20.87 ± 2.31 mV and shifted to −11.40 ± 1.51 mV when loading with TPET-probe (Figure 2g). Hydrodynamic size of MoS_2 nanosheets slightly shift to 200–600 nm after TPET-probe loading (Figure 2h) These characterizations verified that the adsorption of MoS_2 nanosheets to the TPET-labeled mononucleotides [21].

3.3 | Feasibility of Exo III-aided MoS_2/AIE nanoprobes for Omicron NA detection

We tested the PL intensity of both bare TPET molecules (dimethyl sulfoxide/water, v/v = 1:199) and TPET-labeled DNA (TPET-DNA), revealing that the PL intensity of TPET-DNA is approximately 17% of that observed for bare TPET (Supporting Information Figure S1). This result supported that TPET-DNA with enhanced hydrophilicity tend to show reduced AIE effect in aqueous environment [20, 31]. Efficient fluorescence quenching of MoS_2 nanosheets and selective cleavage of Exo III in duplex DNAs were the prerequisites for amplified FRET detection. In Figure 3a, the MoS_2 showed wide optical absorbance from 200 to 800 nm and overlapped with the emission of TPET (peak at 650 nm) which ensured the optical basis of FRET sensing. Figure 3b

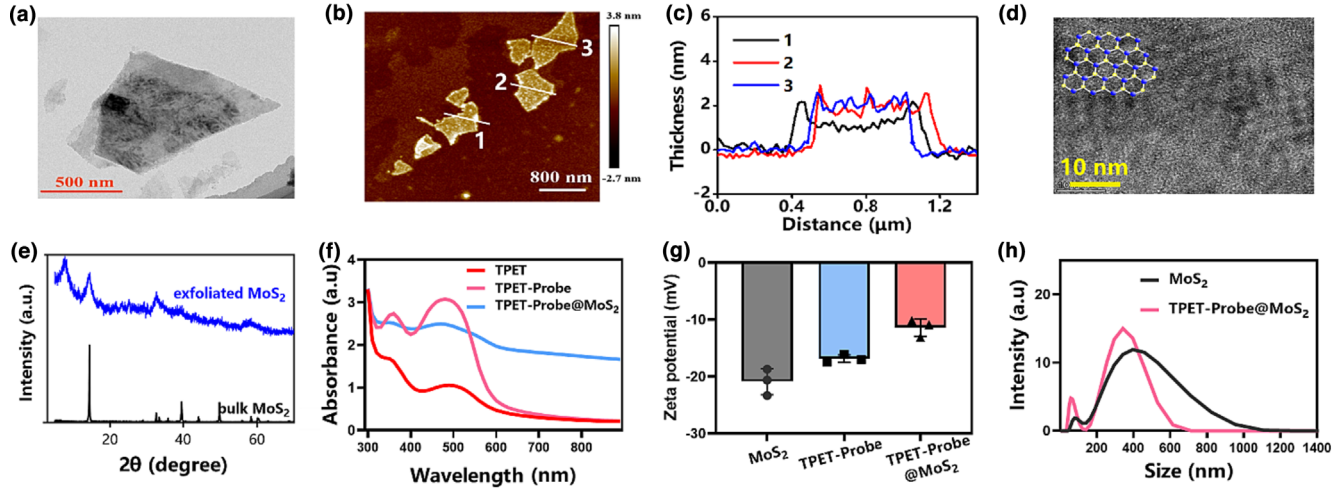

FIGURE 2 (a) TEM morphology of MoS_2 nanosheets; (b,c) AFM analysis of morphology and thickness of thin-layered MoS_2 nanosheets; (d) high-resolution TEM image of MoS_2 nanosheets; (e) XRD patterns of MoS_2 nanosheets; (f) UV-vis absorbance spectra of TPET, TPET-probe, TPET-probe@MoS_2; (g) zeta potentials of MoS_2, TPET-probe, TPET-probe@MoS_2; (h) hydrodynamic size distributions of MoS_2 and TPET-probe@MoS_2.

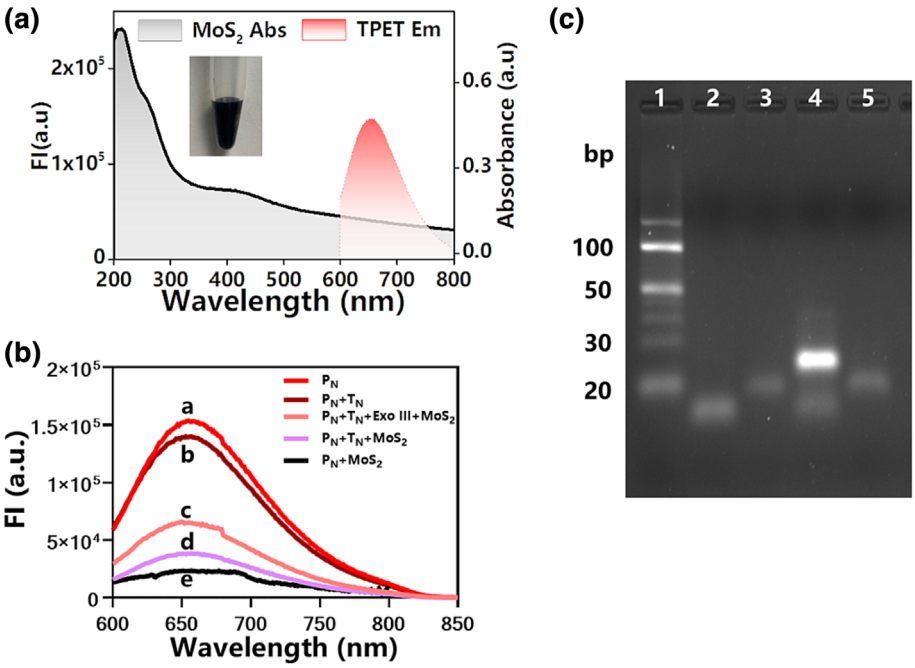

FIGURE 3 (a) UV-vis spectrum of MoS_2 nanosheets and PL emission spectrum of TPET. (b) PL spectra for P_N, $P_N + T_N$, $P_N + T_N + MoS_2$ + with/without Exo III, $P_N + MoS_2$; curve a: P_N (20 nM), curve b: $P_N + T_N$ (20 nM:5 nM), curve c: $P_N + T_N + MoS_2$ + Exo III (20 nM:5 nM:120 μg mL^{-1}:0.015 U μL^{-1}); curve d: $P_N + T_N + MoS_2$ (20 nM:5 nM:120 μg mL^{-1}), curve e: $P_N + MoS_2$ (20 nM:120 μg mL^{-1}). (c) Agarose-gel electrophoresis analysis of samples as: lane 1: 10 bp DNA ladder, lane 2: 400 nM P_N, lane 3: 200 nM T_N, lane 4: 400 nM P_N + 200 nM T_N, lane 5: 400 nM P_N + 200 nM T_N + 0.3 U μL^{-1} Exo III.

demonstrated the feasibility of using Exo III-aided MoS_2/AIE nanoprobes for amplified detection of Omicron NAs. It showed that in the presence of MoS_2 nanosheets (120 μg mL^{-1}), the fluorescence of P_N (20 nM) was quenched obviously (curve e), and the FI of $P_N + T_N + MoS_2$ (curve d) was 1.63-times that of $P_N + MoS_2$ (curve e) because T_N hybridized with P_N and partially triggered the restoration of fluorescence. The role of Exo III in signal amplification was indicated by comparison of the fluorescence for samples of $P_N + T_N + MoS_2$ with and without the aid of Exo III. The Exo III-aided sample (curve c) had 1.74-times higher FI than that of the Exo III-free sample (curve d). This supports the fact that Exo III cleaved the hydrophilic portion of P_N and triggered the aggregation of the released TPET molecules. The fluorescence enhancement is theoretically attributed to the RIR effect of free TPET, where RIR halts nonradiative deactivation pathways, thereby promoting the excited states of the molecules upon light excitation [34, 35]. Selective digestion of Exo III to single-strand P_N in P_N/T_N duplex DNAs was determined by agarose-gel electrophoresis (Figure 3c). Two bright bands representing P_N and T_N were observed in P_N/T_N duplex DNA without Exo III treatment (lane 4). However, bands for P_N in the P_N/T_N duplex DNA after Exo III treatment were not observed (lane 5), which indicated selective digestion by Exo III.

3.4 | Optimization of assay conditions

The assay conditions for MoS_2/AIE-based FRET and Exo-III catalysis were optimized systematically. Initially, to adapt the ratio between the fluorescence donor (TPET) and acceptor (MoS_2 nanosheets), samples with P_N (20 nM) and $P_N + T_N$ (20 nM:5 nM) were treated with Exo III (0.015 U μL^{-1}) and MoS_2 nanosheets (0, 50,100, 120, 135, or 150 $\mu g\ mL^{-1}$). The FI of P_N and $P_N + T_N$ decreased gradually with increasing MoS_2 concentration (Figure 4a). The quenching efficiency (Qe) of $P_N + T_N$ treated with MoS_2 was up to 74.6%, and stable quenching could cover the entire detection time completely. The value of Qe was calculated using the equation $(F_t - F_q)/F_t$, where F_t and F_q represented the FI of samples before and after MoS_2 quenching, respectively. However, redundant MoS_2 (> 120 $\mu g\ mL^{-1}$) caused an excessively dark background and hid the fluorescence signal restored by T_N. The corresponding ratio of FI_{PN+TN}/FI_{PN} reached a maximum of 1.75 in the presence of MoS_2 at 120 $\mu g\ mL^{-1}$ (Figure 4b).

To optimize the catalytic conditions of Exo III, the amount and time needed for Exo III application were investigated further. Samples of $P_N + T_N$ (20 nM:5 nM) were treated with Exo III (0.005, 0.01, 0.015, or 0.02 U μL^{-1}) for 40 min. MoS_2 at 120 $\mu g\ mL^{-1}$ was applied in each group for fluorescence quenching. FI was enhanced progressively with an increase in the amount of Exo III, and reached saturation at 0.015 U μL^{-1} of Exo III (Figure 4c). Excess Exo III (> 0.02 U μL^{-1}) could increase the background noise and saturate the amplified signal [36]. The time needed for Exo III to carry out catalysis was determined by incubating a sample of $P_N + T_N$ (20 nM:5 nM) with Exo III at 0.015 or 120 $\mu g\ mL^{-1}$ for 0, 20, 40, 60, or 100 min. The FI of each group increased gradually with increasing time, and reached saturation at 40 min (Figure 4d).

3.5 | Amplified detection of multiple gene oligos of Omicron

After optimization of sensing conditions, Exo III-aided MoS_2/AIE nanoprobes were applied to identify the deleted N-gene and S-gene oligos of Omicron. A substrate sample of P_N (20 nM) was incubated with Exo III (0.015 U μL^{-1}) and then treated with MoS_2 nanosheets (120 $\mu g\ mL^{-1}$) to detect T_N (0, 0.01, 0.05, 0.1, 0.15, 0.3, 0.5, 1.0, 1.5, 2.5, or 5.0 nM). The relative FI was calculated by the equation $(F_t - F_{nt})/F_{nt}$, where F_t and F_{nt} represented the FI of the substrate sample with and without target oligos, respectively. The fluorescence spectrum was characterized by emission from 600 nm to 850 nm after excitation at 480 nm (Figure 5a). The relative FI increased gradually with increasing T_N concentration at a linear range from 0.01 to 0.5 nM, in which the LOD was 4.7 pM (Figure 5b). Herein, LOD was calculated by $3\sigma/S$. We applied the same assay conditions to quantitatively detect the second target, Ts, which resulted in the LOD of 6.8 pM (Figure S2A,B). The analytical performance of Exo III-aided MoS_2/AIE nanoprobes was compared with that of recently reported enzyme-assisted nanosensors for NA detection (Table 1). The sensing method applied in this work exhibited higher sensitivity and comparable time for detection than most reported methods. In conventional Exo III-assisted FRET assays, the fluorescence signal of the restored fluorescence dyes is prone to decrease due to the ACQ effect. However, Exo III cleavage transitions the dispersed state of AIE, thereby triggering the enhancement of fluorescence signals [31, 47].

Sensing specificity of T_N and T_S by Exo III-aided MoS_2/AIE nanoprobes was undertaken (Figure 5c). A distinguishable fluorescence signal could be collected only in the presence of the specific T_N or T_S targets without suffering interference by other

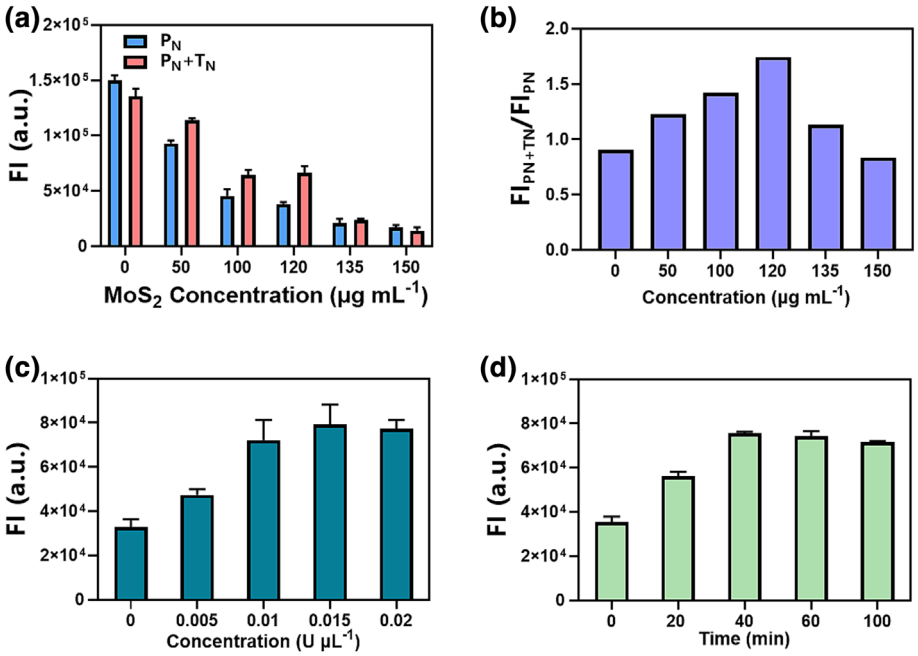

FIGURE 4 (a) FI of P_N (20 nM) and $P_N + T_N$ (20: 5 nM) treated with 0.015 U μL^{-1} Exo III and incubated with 0, 50, 100, 120, 135, 150 $\mu g\ mL^{-1}$ MoS_2 nanosheets. (b) Ratio of FI_{PN+TN}/FI_{PN} analyzed for P_N and $P_N + T_N$ treated with different concentrated MoS_2. (c) FI for T1 detection by treating $P_N + T_N$ samples with 0, 0.5, 1, 1.5, 2 U of Exo III and incubated with 120 $\mu g\ mL^{-1}$ MoS_2. (d) Catalyzation time of Exo III analysis by treating $P_N + T_N$ with 0.015 U μL^{-1} Exo III at 37°C for 0, 20, 40, 60, and 100 min.

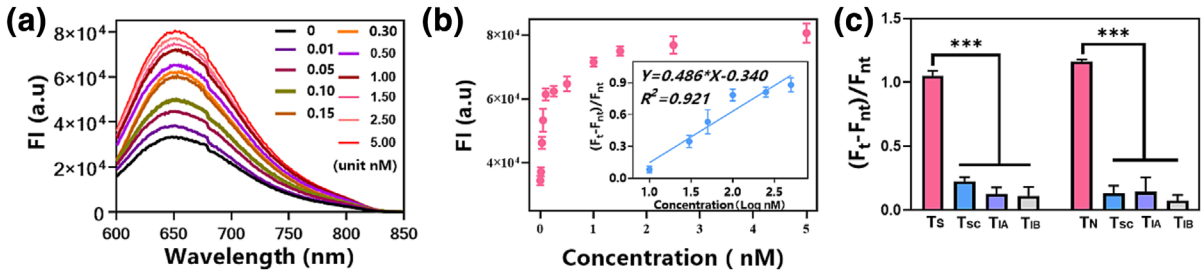

FIGURE 5 (a) Fluorescence spectra of Exo-III-aided MoS_2/AIE FRET nanoprobes for T_N detection. (b) The relationship between $(F_t - F_{nt})/F_{nt}$ and the concentration of T_N (0–5 nM); insert: the plot of $(F_t - F_{nt})/F_{nt}$ versus the logarithm concentration of T_N (0.01–0.5 nM) ($n = 3$, mean ± standard deviation). (c) Specificity detection of Exo III-aided MoS_2/AIE nanoprobes for T_N/T_S targets, and non-target oligos of scrambled target (T_{SC}), M gene of Influenza-A (T_{IA}), HA gene of Influenza-B (T_{IB}) (concentration of all targets and non-targets oligos was 1.0 nM) ($n = 3$, mean ± standard deviation, ***$P < 0.001$, P-value was calculated by Student t-test).

TABLE 1 Comparison of reported methods with that of exonuclease III (Exo III)-aided molybdenum disulfide/aggregation-induced emission (MoS_2/AIE)-based sensing method.

Applied nanomaterial and reference	Target gene	Multi-target (yes/no)	Applied enzyme	Reaction time	LOD
Gold nanoparticles (AuNPs) [37]	miRNA-let 7b/200b/21	Yes	DNaseI/ Exo III	120 min	N/A
Molybdenum disulfide/quantum dots (MoS_2/QDs) [38]	miRNA-21	No	DNase I	30 min	0.5 pM
ZnS:Mn^{2+} QDs [39]	Polynucleotide kinase	No	λ Exo	45 min	2.8 ng mL^{-1}
Graphene oxide (GO) [29]	DNA	No	Exo III	40 min	0.5 pM
Titanium carbide (Ti_3C_2) nanosheets [40]	Human papillomavirus genes	No	Exo III	60 min	100 pM
AuNPs [41]	Hairpin oligonucleotide	Yes	Exo III	120 min	0.13 nM
AuNPs [42]	Nucleic acids	No	Exo III	12 h	10 fM to 200 pM
GO nanosheets [43]	Ochratoxin A	No	Exo III	40 min	0.96 nM
Mesoporous silica [44]	Adenosine triphosphate	No	Exo III	120 min	0.1 nM
GO nanosheets [45]	Adenosine triphosphate	No	Exo III	60 min	0.08 mg mL^{-1}
MoS_2 nanosheets [46]	Human immune deficiency virus DNA	No	Exo III	30 min	5.3 pM
MoS_2 nanosheets (this work)	Deleted genes of Omicron	Yes	Exo III	40 min	4.7 pM

targets. The specificity of T_N detection was studied by incubating Exo III-aided MoS_2/AIE nanoprobes with T_N and various non-target sequences (T_{SC}, T_{IA}, T_{IB}). The specificity of T_S detection was analyzed under the conditions stated earlier. Exo III-aided MoS_2/AIE nanoprobes showed good specificity to the deleted N genes and S genes of Omicron, with at least 4.6- and 8.7-times of fluorescence signal than that of the non-target samples.

4 | CONCLUSIONS

We presented a sensitive, rapid, and inexpensive sensing strategy for detection of the NAs of Omicron based on Exo III-aided MoS_2/AIE nanoprobes. Our method leveraged the flexible affinity of MoS_2 nanosheets to ssDNA and duplex DNAs, luminescent characteristics of AIE, as well as the catalytic activity of Exo III to demonstrate a readily operatable amplification assay. Due to the excellent optical properties of AIE and 2D MoS_2 nanosheets, the nanoprobes enabled efficient detection of multiple targets of the deleted N genes and S genes of Omicron. Here, we propose a sensing concept for detection of short-chain viral NAs. Based on this concept, this probe has the potential for simultaneous detection of multiple targets by combining different fluorescent AIE molecules and capture genes in the future. The short-chain viral NA detection based on this nanoprobe has a low cost and may be more suitable for large-scale community testing. However, due to the limited adsorption capability of 2D nanosheets on long-chain capture genes, there are still restrictions on using the nanoprobes for detecting long-chain viral NAs [48, 49]. This low-cost, high-efficiency sensing method based on nanomaterials has good potential in applications of clinical and community medicine.

AUTHOR CONTRIBUTIONS

Gerile Oudeng: conceptualization; methodology; experimental; data curation; and writing (preparation of original draft). **Junguo Ni:** methodology; experimental; data curation; and data visualization. **Hao Wu and Honglian Wu:** data curation; data visualization; and writing (preparation of original draft). **Mo Yang and Chun yi Wen:** investigation and project administration. **Yuanwei Wang and Hui Tan:** conceptualization; supervision; funding acquisition; and writing (review and editing).

CONFLICT OF INTEREST STATEMENT

The authors declare that they have no known competing financial interests or personal relationships that could have influenced the work reported in this article.

DATA AVAILABILITY STATEMENT

Data available on request from the authors.

ORCID

Yuanwei Wang https://orcid.org/0000-0002-2959-7715

REFERENCES

[1] https://covid19.who.int/
[2] https://covariants.org/
[3] O. Erster, A. Beth-Din, H. Asraf, V. Levy, A. Kabat, B. Mannasse, R. Azar, O. Shifman, S. Lazar, M. Mandelboim, S. Fleishon, E. Mendelson, N.S. Zuckerman, Specific detection of SARS-COV-2 B.1.1.529 (Omicron) variant by four RT-qPCR differential assays, medRxiv. (**2021**) *1*. https://doi.org/10.1101/2021.12.07.21267293
[4] F. Zeng, Y. Huang, Y. Guo, M. Yin, X. Chen, L. Xiao, G. Deng, *Int. J. Infect. Dis.* **2020**, *96*, 467. https://doi.org/10.1016/j.ijid.2020.05.055
[5] G. Seo, G. Lee, M. J. Kim, S. H. Baek, M. Choi, K. B. Ku, C. S. Lee, S. Jun, D. Park, H. G. Kim, S. J. Kim, J. O. Lee, B. T. Kim, E. C. Park, S. I. Kim, *ACS Nano* **2020**, *14*(4), 5135. https://doi.org/10.1021/acsnano.0c02823
[6] A. Yakoh, U. Pimpitak, S. Rengpipat, N. Hirankarn, O. Chailapakul, S. Chaiyo, *Biosens. Bioelectron.* **2021**, *176*, 112912. https://doi.org/10.1016/j.bios.2020.112912
[7] P. Fathi-Hafshejani, N. Azam, L. Wang, M. A. Kuroda, M. C. Hamilton, S. Hasim, M. Mahjouri-Samani, *ACS Nano* **2021**, *15*(7), 11461. https://doi.org/10.1021/acsnano.1c01188
[8] Z. Zhan, J. Li, Z. J. Cheng, *J Epidemiol Glob Health* **2022**, *12*(1), 13. https://doi.org/10.1007/s44197-021-00030-4
[9] Z. Song, Y. Ma, M. Chen, A. Ambrosi, C. Ding, X. Luo, *Anal. Chem.* **2021**, *93*(14), 5963. https://doi.org/10.1021/acs.analchem.1c00724
[10] X. Zhu, X. Wang, L. Han, T. Chen, L. Wang, H. Li, S. Li, L. He, X. Fu, S. Chen, *Biosens. Bioelectron.* **2020**, *166*, 112437. https://doi.org/10.1016/j.bios.2020.112437
[11] G. Qiu, Z. Gai, Y. Tao, J. Schmitt, G. A. Kullak-Ublick, J. Wang, *ACS Nano* **2020**, *14*(5), 5268. https://doi.org/10.1021/acsnano.0c02439
[12] Q. Zhang, B. Yin, J. Hao, L. Ma, Y. Huang, X. Shao, C. Li, Z. Chu, C. Yi, S. H. D. Wong, *Aggregate* **2023**, *4*(1), e195. https://doi.org/10.1002/agt2.195
[13] G. Oudeng, M. Benz, A. A. Popova, Y. Zhang, C. Yi, P. A. Levkin, M. Yang, *ACS Appl. Mater. Interfaces* **2020**, *12*(50), 55614. https://doi.org/10.1021/acsami.0c16146
[14] X. Qiu, N. Hildebrandt, *Expert Review of Molecular Diagnostics* **2019**, *19*(9), 767. https://doi.org/10.1080/14737159.2019.1649144
[15] D. Feng, M. Ren, Y. Miao, Z. Liao, T. Zhang, S. Chen, K. Ye, P. Zhang, X. Ma, J. Ni, X. Hu, H. Li, J. Peng, A. Luo, L. Geng, Y. Deng, *Biosens. Bioelectron.* **2022**, *207*, 114112. https://doi.org/10.1016/j.bios.2022.114112
[16] Z. Wang, J. Huang, J. Huang, B. Yu, K. Pu, F.-J. Xu, *Aggregate* **2021**, *2*(6), e140. https://doi.org/10.1002/agt2.140
[17] J. Luo, Z. Xie, J. W. Lam, L. Cheng, H. Chen, C. Qiu, H. S. Kwok, X. Zhan, Y. Liu, D. Zhu, B. Z. Tang, *Chem. Commun.* **2001**, *18*, 1740. https://doi.org/10.1039/b105159h
[18] C. Y. K. Lam, Q. Zhang, B. Yin, Y. Huang, H. Wang, M. Yang, S. H. D. Wong, *J. Compos. Sci.* **2021**, *5*(7), 190. https://doi.org/10.3390/jcs5070190
[19] H. Noguchi, Y. Nakamura, S. Tezuka, T. Seki, K. Yatsu, T. Narimatsu, Y. Nakata, Y. Hayamizu, *ACS Appl. Mater. Interfaces* **2023**, *15*(11), 14058. https://doi.org/10.1021/acsami.2c23227
[20] Q. Zhang, B. H. Yin, Y. Huang, Y. Gu, J. Yan, J. Chen, C. Li, Y. Zhang, S. H. D. Wong, Y. Mo, *Biosens. Bioelectron.* **2023**, *230*, 115270. https://doi.org/10.1016/j.bios.2023.115270
[21] G. Oudeng, M. Au, J. Shi, C. Wen, Y. Mo, *ACS Appl. Mater. Interfaces* **2018**, *10*(1), 350. https://doi.org/10.1021/acsami.7b18102
[22] J. Qian, H. Cui, X. Lu, C. Wang, K. An, N. Hao, K. Wang, *Chem. Eng. J.* **2020**, *401*, 126017. https://doi.org/10.1016/j.cej.2020.126017
[23] X. Sun, C. Chen, C. Xiong, C. Zhang, X. Zheng, J. Wang, X. Gao, Z. Yu, Y. Wu, *Nano Res.* **2023**, *16*(1), 917. https://doi.org/10.1007/s12274-022-4802-8
[24] Y. J. Wang, Y. Shi, Z. Wang, Z. Zhu, X. Zhao, H. Nie, J. Qian, A. Qin, J. Z. Sun, B. Z. Tang, *Chem—Eur. J.* **2016**, *22*(28), 9784. https://doi.org/10.1002/chem.201600125
[25] C. Chen, X. Xiang, Y. Liu, G. Zhou, X. Ji, Z. He, *Biosens. Bioelectron.* **2014**, *58*, 205. https://doi.org/10.1016/j.bios.2014.02.060
[26] D. Y. Ryazantsev, D. A. Tsybulsky, I. A. Prokhorenko, M. V. Kvach, Y. V. Martynenko, P. M. Philipchenko, V. V. Shmanai, V. A. Korshun, S. K. Zavriev, *Anal. Bioanal. Chem.* **2012**, *404*(1), 59. https://doi.org/10.1007/s00216-012-6114-4
[27] Q. Guo, X. Yang, K. Wang, W. Tan, W. Li, H. Tang, H. Li, *Nucleic Acids Res.* **2009**, *37*(3), e20. https://doi.org/10.1093/nar/gkn1024
[28] C. D. Mol, C. F. Kuo, M. M. Thayer, R. P. Cunningham, J. A. Tainer, *Nature* **1995**, *374*(6520), 381. https://doi.org/10.1038/374381a0
[29] L. Peng, Z. Zhu, Y. Chen, D. Han, W. Tan, *Biosens. Bioelectron.* **2012**, *35*(1), 475. https://doi.org/10.1016/j.bios.2012.03.002
[30] C. Zhu, Z. Zeng, H. Li, F. Li, C. Fan, H. Zhang, *J. Am. Chem. Soc.* **2013**, *135*(16), 5998. https://doi.org/10.1021/ja4019572
[31] R. Zhang, R. T. Kwok, B. Z. Tang, B. Liu, *RSC Adv.* **2015**, *5*(36), 28332. https://doi.org/10.1039/C5RA00322A
[32] Y. Li, R. T. Kwok, B. Z. Tang, B. Liu, *RSC Adv.* **2013**, *3*(26), 10135. https://doi.org/10.1039/C3RA41983E
[33] S. Ding, D. Zhang, J. S. Chen, X. W. Lou, *Nanoscale* **2012**, *4*(1), 95. https://doi.org/10.1039/c1nr11552a
[34] M. Kang, Z. Zhang, N. Song, M. Li, P. Sun, X. Chen, D. Wang, B. Z. Tang, *Aggregate* **2020**, *1*(1), 80. https://doi.org/10.1002/agt2.7
[35] H. Yan, Y. He, D. Wang, T. Han, B. Z. Tang, *Aggregate* **2023**, *4*(4), e331. https://doi.org/10.1002/agt2.331
[36] L. Lu, X. Han, J. Lin, Y. Zhang, M. Qiu, Y. Chen, M. Li, D. Tang, *Analyst* **2021**, *146*(8), 2664. https://doi.org/10.1039/d1an00178g
[37] S. Bai, B. Xu, Y. Guo, J. Qiu, W. Yu, G. Xie, *Theranostics* **2018**, *8*(9), 2424. https://doi.org/10.7150/thno.23852
[38] X. Yu, L. Hu, F. Zhang, M. Wang, Z. Xia, W. Wei, *Microchim. Acta* **2018**, *185*(4), 239. https://doi.org/10.1007/s00604-018-2773-y
[39] G. Jie, C. Li, Y. Zhao, Q. Kuang, S. Niu, *ACS Appl. Nano Mater.* **2019**, *2*(7), 4637. https://doi.org/10.1021/acsanm.9b01003
[40] X. Peng, Y. Zhang, D. Lu, Y. Guo, S. Guo, *Sens. Actuators B Chem.* **2019**, *286*, 222. https://doi.org/10.1016/j.snb.2019.01.158
[41] C. Kong, L. Gao, Z. Chen, *Microchim. Acta* **2018**, *185*(10), 488. https://doi.org/10.1007/s00604-018-3031-z

[42] X. Qu, D. Zhu, G. Yao, S. Su, J. Chao, H. Liu, X. Zuo, L. Wang, J. Shi, W. Huang, H. Pei, C. Fan, *Angew. Chem., Int. Ed.* **2017**, *56*(7), 1855. https://doi.org/10.1002/anie.201611777
[43] M. Liu, X. Li, B. Li, J. Du, Z. Yang, *Microchim. Acta* **2019**, *187*(1), 46. https://doi.org/10.1007/s00604-019-3992-6
[44] X. Li, Y. Wang, J. Luo, S. Ai, *Sens. Actuators B Chem.* **2016**, *228*, 509. https://doi.org/10.1016/j.snb.2016.01.082
[45] C. Wen, Y. Huang, J. Tian, K. Hu, L. Pan, S. Zhao, *Anal Methods-UK* **2015**, *7*(9), 3708. https://doi.org/10.1039/C5AY00354G
[46] L. Wang, L. Dong, G. Liu, X. Shen, J. Wang, C. Zhu, M. Ding, Y. Wen, *Microchim. Acta* **2019**, *186*(5), 286. https://doi.org/10.1007/s00604-019-3368-y
[47] T. Zhou, Q. Wang, M. Liu, Z. Liu, Z. Zhu, X. Zhao, W. Zhu, *Aggregate* **2021**, *2*(2), e22. https://doi.org/10.1002/agt2.22
[48] Y. Huang, H. Y. Hui, Y. Ai, *Anal. Chem.* **2015**, *87*(18), 9132. https://doi.org/10.1021/acs.analchem.5b03037
[49] M. Wu, R. Kempaiah, P. J. Huang, V. Maheshwari, J. Liu, *Langmuir* **2011**, *27*(6), 2731. https://doi.org/10.1021/la1037926

SUPPORTING INFORMATION

Additional supporting information can be found online in the Supporting Information section at the end of this article.

How to cite this article: G. Oudeng, J. Ni, H. Wu, H. Wu, M. Yang, C. Wen, Y. Wang, H. Tan, *Luminescence* **2024**, *39*, e4675. https://doi.org/10.1002/bio.4675